Collisional excitation transfer in high magnetic fields. III. Potential symmetry rules and correlation function in Na(3^2P_J)-Na($3^2S_{1/2}$) collisions

J. C. Gay and W. B. Schneider*

Laboratoire de Spectroscopie Hertzienne de l'E.N.S., Tour 12, Université Pierre et Marie Curie, 4 Place Jussieu, 75320 Paris Cedex 05, France †

(Received 1 August 1978)

An experimental study of excitation transfer between certain Zeeman sublevels of the 3^2P_J states in strong magnetic fields is reported for Na($3^2S_{1/2}$)-Na*(3^2P_J) resonant collisions. A major decrease in the $M = -3/2 \rightarrow M = 3/2$ transfer rate is observed between 4 and 80 kG. Approximate calculations in the correlation-function framework are performed, and the experimental results and theoretical predictions for the field dependence are in good agreement. Some insights into the mechanisms of the collision process are deduced and the particularly important role of the electronic spin is emphasized. The importance of the symmetry properties of the interaction potential is also directly demonstrated.

I. INTRODUCTION

The principle of these experiments on the $(3^2P_{1/2,3/2})$ fine-structure levels of sodium is analogous to that described for mercury atoms in a previous paper.[1] In essence, we excite one (J, M_J) level and observe the collisionally induced fluorescence intensities from the (J', M'_J) levels. This method has frequently been used to study excitation transfer due to noble-gas collisions and to alkali-metal-gas collisions in low magnetic fields.[1(c)] Here we study the dependence of these cross sections on magnetic field in a region where the Zeeman energy splittings are of sufficient magnitude to make the collisions partially adiabatic. An experimental determination of the Fourier transform of the correlation function for the interaction potential is then possible.

Some difference exist between the present experiment and that of Ref. 1, concerning both the experimental procedure and the interpretation of the data. Excitation by a tunable dye laser is necessary in the present experiment, as all the Zeeman components of the resonance lines are displaced by the magnetic field. This offers the possibility of measuring, by frequency and polarization analysis of the fluorescent light, the whole ensemble of transfer coefficients between the various Zeeman sublevels. But the interpretation of the experiments is more complicated than in the mercury case because of the existence of the hyperfine structure, the nonzero electronic spin of the ground state, and the partial LS decoupling in the excited state due to the field.

When one neglects the role of symmetry properties, which are of interest for small LS decoupling effects, there are 132 independent coefficients of transfer in Na-Na* resonant collisions. Indeed, 12 of these can be deduced from the unitarity of the S matrix.

Experimental investigations of the whole set of coefficients are possible if one creates polarized perturbers in the ground state. But in our conditions we use thermalized ground-state atoms and we can only experimentally investigate the behavior of the average value of the transfer coefficients on the ground state. The number of possible coefficients investigated with unpolarized perturbers and optical detection of the excited state is then reduced to 30. Among these are many uninteresting or small ones in fields smaller than 80 kG, as, for example, those describing fine-structure transfer processes which may be measured but with a poor accuracy.

In the following, the rates of transfer between the states of the two-atom system, i.e., $[\tilde{J}M_J, j = \frac{1}{2}m \rightarrow j = \frac{1}{2}m', \tilde{J}'M'_{J'}]$ will be denoted by $[JM_J m \rightarrow J'M'_{J'}, m']$ or $[JM_J \rightarrow J'M'_{J'}]$ when averaging over m, m' (in the vapor) is assumed.

Our experimental investigations have been restricted to the $(\frac{1}{2} - \frac{1}{2} \rightarrow \frac{1}{2}\,\frac{1}{2})$ and $(\frac{3}{2} - \frac{3}{2} \rightarrow \frac{3}{2}\,\frac{3}{2})$ processes. The $(\frac{3}{2} - \frac{3}{2} \rightarrow \frac{3}{2} \pm \frac{1}{2})$ processes have also been observed, but with a poor signal-to-noise ratio, which permits only qualitative conclusions. The study of other processes would be of interest, particularly for testing the validity of symmetry properties, but in fact this requires the use of a detailed comparison theory requiring major numerical work. It would also be of interest to study excitation transfer between fine-structure Zeeman sublevels in higher fields, as the transfer should increase strongly up to the crossing points in the vicinity of 164 and 250 kG, as shown in Sec. VII.

II. EXPERIMENTAL SETUP

The apparatus is shown in Fig. 1. The resonance cell is at the center of a superconducting magnet which produces fields of up to 80 kG.[1] The cells are cylindrical Pyrex chambers of 10-cm length and 2-cm diameter, connected to a pumping line in order to avoid troubles due to residual gases,

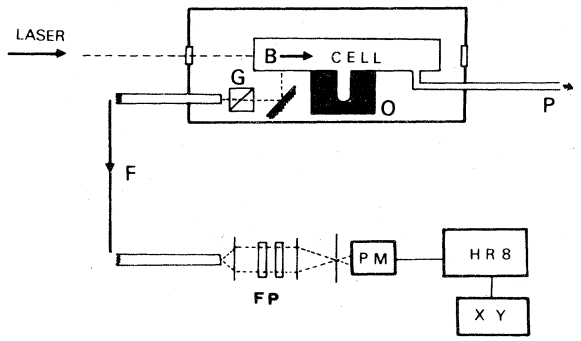

FIG. 1. Experimental apparatus: O represents the oven, P the pumping line, G the Glan-type polarizer, F the flexible light guide, FP the Fabry-Perot interferometer. The chopped σ-polarized laser beam is sent in the field direction and detected at right angles to B. Prior to any experiment, it was ensured that scattered excitation light did not exceed 10^{-3} of the fluorescent light.

which may severely perturb such experiments.[1] Some attempts made with sealed silica and Pyrex cells revealed the presence of about 10^{-3} Torr residual-gas pressures at low temperature. The cell is placed in an oven the temperature of which is kept constant within 10^{-2} °C by an oil-circulating system connected to an external thermostat. A water cooling system isolates the 500-°K oven from the cryostat of the magnet.

The light source is an Ar^+-pumped R6G multimode jet-stream dye laser. Wavelengths are selected with a Lyot filter and a thin 1-mm silica slab of variable inclination inside the cavity. The bandwidth of the laser is about 4 GHz with three modes. Short-term frequency instabilities caused by mode competition during the integration time of the detection system insure a quasi-broad-line excitation of the chosen Zeeman substate. The linewidth of one Zeeman component is about 3 GHz at 500 °K owing to hyperfine structure (which is not resolved in the experiments) and Doppler effect. For fields greater than 4 kG the Zeeman splitting is large enough to allow selective excitation of only one Zeeman substate of the 3^2P_J levels. A coated variable-absorption slab is used to verify that the data are free from nonlinear effects or optical pumping of the ground-state atoms, which is highly improbable as the power incident on the cell is only a few milliwatts in a 5-mm-diam beam.

The excitation of the sodium vapor is performed with a chopped laser beam, the direction of which is parallel to the magnetic field. The σ-fluorescence light is detected at a right angle to the field direction with a Glan-type polarizer, and sent by means of an optical fiber to two thermostabilized piezoelectrically scanned Fabry-Perot interferometers (FP) for frequency analysis.

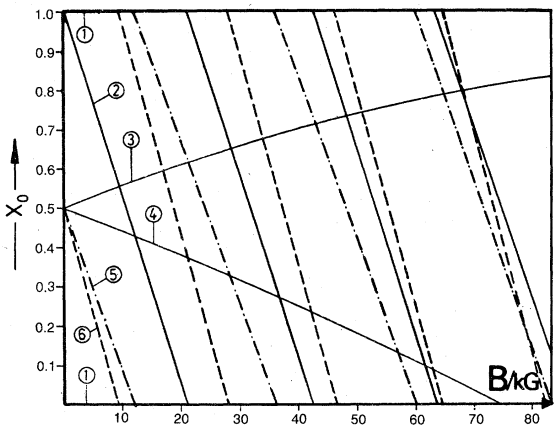

FIG. 2. Calculated pattern of the interferometer showing the overlap of the interference orders of the six σ lines (3^2P states) as a function of the magnetic field strength. The mirror distance of the Fabry-Perot interferometer is set at 0.189 cm. The plot gives the relative positions X_0 of the lines in units of the interferometer free-spectral range. The numbers correspond to the σ lines associated with the following Zeeman substates: (1) $^2P_{1/2\,-1/2}$, (2) $^2P_{1/2\,1/2}$, (3) $^2P_{3/2\,-1/2}$, (4) $^2P_{3/2\,-3/2}$, (5) $^2P_{3/2\,3/2}$, and (6) $^2P_{3/2\,1/2}$. Overlapping at various field values shows the necessity of using a second interferometer with different free-spectral range.

The polarizer suppresses the π-fluorescence components. In the fields used the electronic and nuclear angular momenta of the $3P$ level are completely decoupled; thus there are only six $\Delta m_J = \pm 1$ or σ-Zeeman components. But as Na-Na* fine-structure transitions are negligible[2,3] at low field values, there are actually only two or four strong-fluorescence lines for the respective cases of $J = \frac{1}{2}$ or $\frac{3}{2}$ excitation.

The free spectral ranges of the interferometers, of finesse $f \simeq 40$, are chosen to obtain the least overlap of Zeeman components over the 0–80-kG range of magnetic field. For the present experiments they were 2.65 and 3.82 cm^{-1}, giving the pattern of Fig. 2. The FP's are followed by a 135-mm-focal-length lens and a 1-mm-diam hole at its focal point. The resulting instrumental width is 3 GHz (2 GHz for the FP and 0.9 GHz for the collimation system). The signal is detected with a shielded water-cooled EMI photomultiplier, sent to a photon-counting system and an Intertechnique averager, and then printed and punched.

III. ORDERS OF MAGNITUDE, CONDITIONS OF STUDY

The experimental conditions adopted for these experiments on sodium are similar to those for mercury.[1,4] But the probability of radiative decay of the resonance level is stronger than that of the 6^3P_1 state of mercury, resulting in a larger reson-

ance interaction and greater cross sections. Also, there are no experimental constraints due to residual gases in the present case.

A. Orders or magnitude of transfer rates in Na-Na* collisions

The radiative decay probability Γ for the $3\,^2P_J$ resonance levels is 6.25×10^7 sec^{-1}. The absorption coefficient $\chi(\frac{3}{2})$ at the center of the $J=\frac{3}{2}\rightarrow j=\frac{1}{2}$ line (neglecting hfs) is given by

$$\chi(\tfrac{3}{2})=\pi^{3/2}2\Gamma N/k_0^3 u\,, \tag{1}$$

with $u=(2kT/M)^{1/2}$, giving for $T=500$ °K and $N=2\times10^{12}$ atoms/cm^3

$$\chi(\tfrac{3}{2})\simeq 19\ \text{cm}^{-1},\quad \chi(\tfrac{1}{2})\simeq 9.6\ \text{cm}^{-1}.$$

The collisional transfer rates can be deduced from the theoretical results of Ref. 5 and have the general form

$$g=2.24\,K\times10^{-15}\Gamma N\,, \tag{2}$$

where K is a quantity of order of unity which depends on the particular Zeeman transition under investigation. For example, for the $m=-\frac{3}{2}\rightarrow m=+\frac{3}{2}$ excitation transfer rate, K deduced from[5] is 0.611. One then obtains for $N=2\times10^{12}$ at./cm^3, a $g^{3/2-3/2}$ value of $2.7\times10^{-3}\Gamma$, very similar to the values used in the experiments on Hg.

The main problem is still multiple scattering of resonance radiation. The excitation is transferred by resonant Na-Na* collisions from the optically excited Zeeman sublevel m_0 towards all the m Zeeman sublevels of the excited state, giving after frequency analysis a pattern such as that of Fig. 3. If the terms corresponding to the back-transfer of excitation from m to m_0 or m to m' are neglected, the expression of the ratio of the detected fluorescence intensities is just proportional to the collisional transfer rate and to the imprisonment time $[\Gamma(m)]^{-1}$ of the excitation in the m sublevel

$$I_m/I_{m_0}\sim\lambda^{mm_0}g^{mm_0}/\Gamma(m)\,. \tag{3}$$

The evaluation of $\Gamma(m)$ with Holstein's model[6] gives for $T=500$ °K, $N=2\times10^{12}$ at./cm^3, $L\simeq7$ cm, and for the $J=\frac{3}{2}$ level the value $\Gamma/\Gamma(m)\sim27$. Then I_m/I_{m_0} is about 0.07, but in fact depends slightly on the process under consideration. Under such conditions, $\Gamma(m)\gg g^{mm_0}$ and the neglect of back-transfer terms is justified. Thus I_m/I_{m_0} is linearly dependent on g^{mm_0} for densities of about 2×10^{12} at./cm^3. As the residual-gas pressure is very low ($<10^{-6}$ Torr), experiments at low temperatures are possible, but practical limitations come from the signal-to-noise ratio and from the necessity of correcting the results from the interferometer function. It is thus necessary to obtain values of I_m/I_{m_0} greater than a few 10^{-2} at least.

B. Order of magnitude of critical fields

As will be shown in the following sections there are several excitation transfer processes with various energy differences between the levels of the two-atom system contributing to the $m_0\rightarrow m$ process in the excited state.[4] The definition of a critical field value for which $\Delta E\tau_c\sim\hbar$ cannot be systematic. Writing $\omega=\mu_B B/\hbar$ for the Larmor frequency, one can show (see Sec. VII) that the $m=-\frac{3}{2}\rightarrow m=\frac{3}{2}$ process evolves at only one characteristic frequency, 2ω, with the field. For this process, the critical field value B_c is given by

$$B_c=(2\mu_B\tau_c)^{-1} \tag{4}$$

and for $T=500$ °K, $\tau_c=(1/v)(\sigma/\pi)^{1/2}$, and $\sigma=8400$ Å^2 this gives $\tau_c=6\times10^{-12}$ sec and $B_c\simeq6$ kG.

C. Conditions of study

The m_0 Zeeman sublevel is selectively and continuously laser excited, and σ-fluorescence intensities are detected and frequency analyzed. A typical plot is given in Fig. 3 for the excitation of the $m_0=-\frac{3}{2}$ Zeeman sublevel. For a fixed Na density, the field is varied between 4 and 80 kG. The ratio I_m/I_{m_0} is then obtained and corrected for interferometer function. For such values of the density and magnetic field, two sweeps of the interferometers are made in order to control the reproductibility of the pattern. Laser power fluctuation during one sweep is less than 1%. The range of densities used is 2×10^{12}–5×10^{12} at./cm^3. A typical plot of the ratio $I^{3/2}/I^{-3/2}$ versus the field is given in Fig. 4. No measurements have

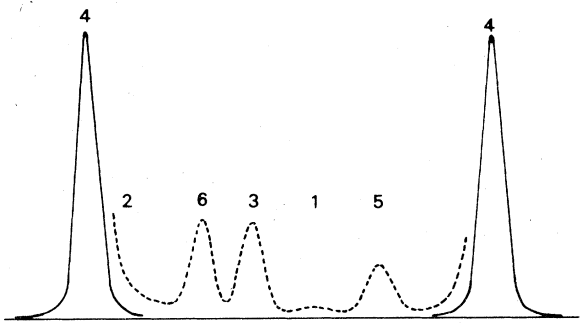

FIG. 3. Typical fluorescence pattern obtained for excitation of the $M=-\frac{3}{2}$ Zeeman sublevel. The free-spectral range of the interferometer is 2.65 cm^{-1}. Sodium density is $N=4\times10^{12}$ at./cm^3 and the field value is 35.8 kG. The collisionally induced components (dashed) are recorded at a sensitivity ten times greater than the direct component (solid, labeled 4). Component 5 corresponds to the fluorescence line reemitted by the $M=\frac{3}{2}$ Zeeman sublevel (see Fig. 2 for the complete assignment of the lines).

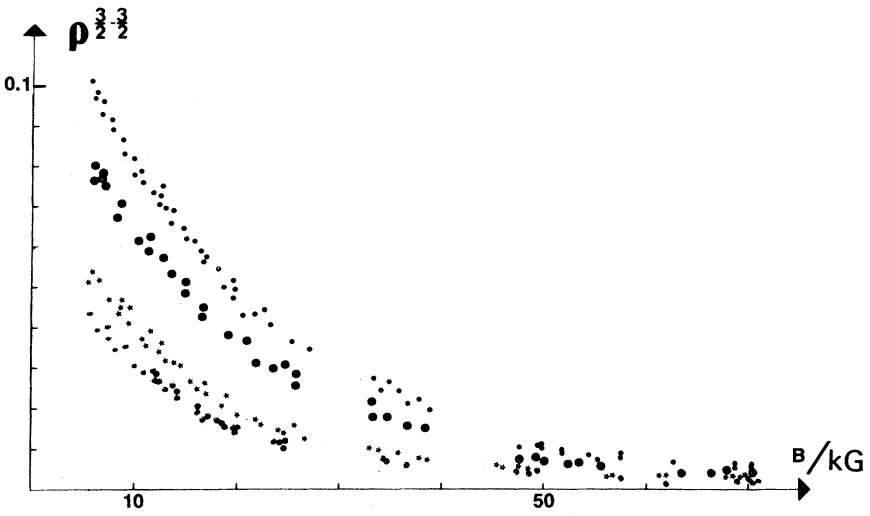

FIG. 4. Variation with field of the ratio $\rho^{3/2,-3/2} = I^{3/2}/I^{-3/2}$ of the fluorescence intensities reemitted by the $M=\frac{3}{2}$ and $M=-\frac{3}{2}$ Zeeman sublevels following excitation of the $J=\frac{3}{2}$ $M=-\frac{3}{2}$ Zeeman sublevel. The values of the density correspond to $N=4.2\times10^{12}$ at./cm^3 (●), 3.8×10^{12} at./cm^3 (✶), and 3.1×10^{12} at./cm^3 (●).

been made around 30 or 42 kG or for fields smaller than 6 kG. This is because of line overlapping with the chosen free spectral ranges of the interferometers.

As in Ref. 1, the radiation trapping times are not accurately known and consequently the absolute determinations of g^{mm_0} is not possible. Nevertheless one can remark that the order of magnitude of the signal we have derived in Sec. IIC are in rather good agreement with the experimental data of Fig. 4.

The low-field data ($B<6$ kG) is, in general, of no practical interest for several reasons. First, one must work in the strong-field regime (i.e., where the Zeeman splitting much greater than the Doppler width) to avoid all depolarization effects due to multiple scattering.[1,7,8] Moreover, the existence of hyperfine structure in the ground and excited states requires working with fields high enough to decouple $\vec{I}$ and $\vec{J}$, and so avoid a trivial parasitic field dependence of the data.[9,10] Fields greater than 4 kG are needed for this purpose. Finally, to selectively excite one Zeeman sublevel and resolve the spectrum of fluorescent light, fields greater than 4 kG are usually needed, depending on the particular process under investigation.

IV. LS DECOUPLING EFFECTS ON MULTIPLE SCATTERING

Interpretation of the data is complicated by the partial decoupling of $\vec{L}$ and $\vec{S}$ due to the field.[11] This results in a field dependence of the parameters of multiple scattering, in particular this forbids any accurate test of the symmetry properties of the collisional relaxation matrix.[12]

A. Isolated excited atom

The $3p$ fine-structure constant is 330 GHz and of the order of magnitude of the magnetic energies for $B\simeq 80$ kG. The energy levels and eigenstates of the Hamiltonian depart from the Zeeman approximation, and the fluorescence intensities reemitted by an isolated excited atom are field dependent.[9,11] Explicit expressions are given in Appendix A, where we show that the probabilities of reemission of σ and π photons by the (JM_J) sublevel vary in opposite ways with the field, the sum of the two probabilities being constant.

At low Na densities ($N\sim10^{10}$ at./cm^3), no radiation trapping occurs and the line intensities depend linearly on the strength of oscillator towards the ground state and on sublevel density. It is then easy to correct the results for decoupling effects as in Ref. 9. But it is not so easy in these Na-Na* collisions studies, since the conditions ($N\sim2\times10^{12}$ at./cm^3) are such that the effects of multiple scattering are not negligible.

B. Decoupling effects and multiple scattering

Multiple scattering is not a linear process, in the sense that line intensities do not depend linearly on the absorption coefficient for a given line.[6,13] The field dependence of the absorption coefficient thus induces a nonlinear field dependence in the intensities reemitted outside the cell. Only qualitative estimations of this are possible.

In the strong-field regime (where the Zeeman splitting is much greater than the Doppler width), the imprisonment of the excitation occurs independently for each Zeeman sublevel M of the excited state, and is characterized by the imprisonment

time $(\Gamma^{(JM)})^{-1}$. The radiative decay of the (JM_J) sublevel can correspond to the emission of σ and π photons, the diffusions of which are deeply entangled and which both contribute to $\Gamma^{(JM)}$. The intensities measured then depend in a rather complicated, unknown way on the magnetic field strength. Some intuitive arguments show that such effects are necessarily weak. First, decoupling effects cause at most 20% variation in the probability of emission in the 0–80-kG range of magnetic field (see Appendix I). Secondly, the probability of emission or absorption of σ and π photons varies in way opposite that of the field strength. Then a partial compensation of the variations occurs, leading to a smooth dependence of $\Gamma^{(JM)}$ on B. At small values of the density, when $\Gamma^{(JM)}$ depends almost linearly on the absorption coefficients, one can always associate two graphs with $(p\sigma, m\pi)$ and $(m\sigma, p\pi)$ photons in a diagrammatic expansion of $\Gamma^{(JM)}$, leading (to first order in B) to an almost complete elimination of the B dependence of $\Gamma^{(JM)}$. At higher values of the density, such a picture is not quite correct, as $\Gamma^{(JM)}$ does not depend linearly on the absorption coefficient.

The last point is that the detected intensities depend on the parameters $\lambda_\sigma(JM)$ and $\lambda_\sigma(J_0M_0)$[1,7,8] (see Sec. V), which are kinds of form factors which depend on the probability of emission of σ photons only. They are also field dependent via decoupling effects, in an unknown way.

Fortunately, there is a situation which permits clear interpretation corresponding to the $J=\frac{3}{2}$ $M=\pm\frac{3}{2}$ Zeeman sublevels not perturbed by the magnetic field. The data are then free of the above-mentioned parasitic-field dependence.

V. FLUORESCENCE INTENSITIES

The evolution of the system under resonant and spin-exchange collisions, multiple scattering, optical pumping, $\vec{L}\cdot\vec{S}$ coupling, and magnetic interactions is described with a two-atom master equation which is nonlinear in the density matrix ρ,[14,15] but solution of this equation in the general case turns out to be difficult. Fortunately in the present case the chosen physical conditions are such that the evolutions of the ground and excited states of the atoms are very simple.

A. Relaxation in ground state

Relaxation in the ground state is due to resonant Na-Na* collisions, Na-Na spin-exchange collisions, wall collisions, and multiple scattering of resonance radiation.[16,17] In spite of the strong oscillator strength of the resonance transition, the rate of optical pumping is no more than 10^2 sec^{-1}, owing to the very small light-power density used in the experiments. This ensures that the density of excited atoms is small compared to that of ground-state atoms.

At the experimental Na densities of 2×10^{12} at./cm^3, the data are free from optical pumping effects on the ground-state sublevels. As the cross section for Na-Na spin-exchange collisions is 1.11×10^{-14} cm^2,[18] the relaxation time is 5×10^{-4} sec, much faster than the optical pumping time. Also, strong radiation trapping effects are responsible for a redistribution of the populations in the ground state. Resonant collisions only weakly affect the ground-state equilibrium since the rates are proportional to the population in the excited state and are thus several orders of magnitude smaller than those for spin-exchange collisions despite greater cross sections.

As the role of the Boltzmann factor is negligible for fields up to 80 kG, the ground-state atoms therefore remain essentially unpolarized.

Remarks. A strong magnetic field may affect the cross sections for spin-exchange collisions in a way analogous to that observed in resonant collisions.[19,20] The main difference lies in the very different orders of magnitude of the cross sections for the two processes. The cross sections for resonant collisions are about 8×10^3 Å^2,[5] while they are only about 2×10^2 Å^2 for spin exchange.[18] The collision times associated with the two processes then differ by one order of magnitude, and the critical fields[12] are in the same ratio. One can then neglect the variation of the cross sections for spin-exchange collisions in the range of fields used for performing the experiments.

B. Master equation for excited atoms

One assumes thermal equilibrium in the ground state, and also that the populations of the excited states are small compared to those of the ground states. The rate equations for the selectively continuously pumped $(j_0m_0 \rightarrow J_0M_0)$ transition with the λ rate are then

$$i\frac{d}{dt}\rho_e^{JM} = -\left(\Gamma^{(JM)} + \sum_{J'M'} g^{(J'M')(JM)}\right)\rho_e^{JM} + \sum_{J'M'} g^{(JM)(J'M')}\rho_e^{J'M'} + \lambda\delta_{JMJ_0M_0}\rho_g^{J_0M_0}, \quad (5)$$

where $\Gamma^{(JM)}$ is the inverse of the imprisonment time of the excitation in the (JM) excited state and the g are resonant-collisional transfer rates.

The steady-state solutions of Eq. (8) are linear in the collision terms only if $\rho_e^{J'M'} \ll \rho_e^{J_0M_0}$ and $\Gamma^{(JM)} \ll \sum_{J'M'} g^{(J'M')(JM)}$, so that

$$\rho_e^{(JM)}/\rho_e^{(J_0M_0)} = g^{(JM)(J_0M_0)}/\Gamma^{(JM)}. \quad (6)$$

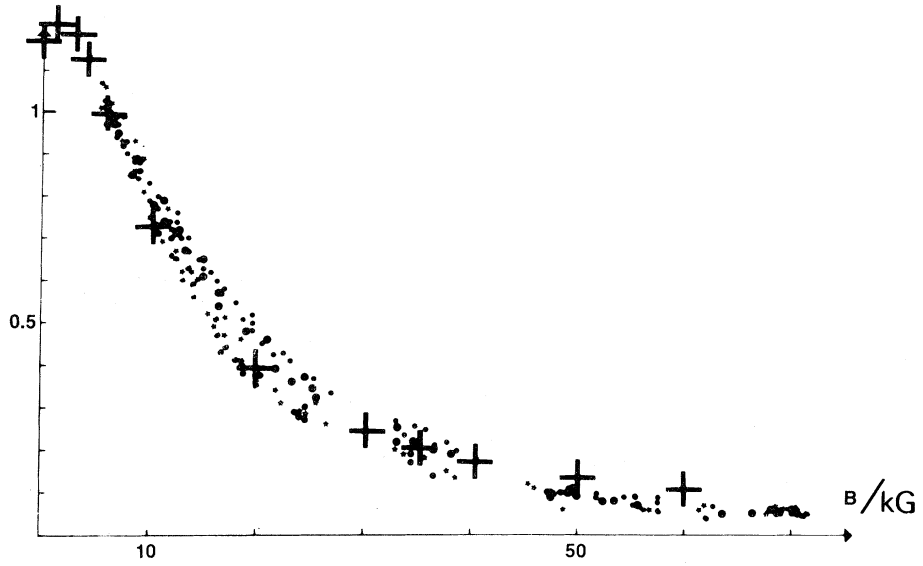

FIG. 5. Variation with the field of $\eta^{3/2-3/2} = \rho^{3/2-3/2}(B) / \rho^{3/2-3/2}(B_0)$ (with $B_0 = 6$ kG) for various density values (the same as in Fig. 4). The theoretical values (+) are those predicted in Sec. VII for $g^{3/2-3/2}(B) / g^{3/2-3/2}(B_0)$.

C. Fluorescence intensities

The σ component of the fluorescence was detected. We assume,[1,7] following the experimental results of a previous paper, that the intensities are just proportional to the mean populations in the vapor. The proportionality factor $\lambda_\sigma(JM)$ depends on the reabsorption probability for σ photons, but also on the radiation diffusion in the cell which deeply entangles the σ and π decays. With (6) one then obtains

$$\rho^{MM_0} = \frac{I^{(JM)}}{I^{(J_0M_0)}} = \frac{\lambda_\sigma(JM)}{\lambda_\sigma(J_0M_0)} \frac{g^{(JM)(J_0M_0)}}{\Gamma^{(JM)}}. \tag{7}$$

Formulation of a detailed theory for the λ's has not been attempted; instead we study the field dependence of this intensity ratio in fields where the λ's are not changing.

VI. EXPERIMENTAL RESULTS

The data obtained at fixed Na density while sweeping the field from 4 to 75 kG have been corrected for the interferometer instrument function.[9] Typical plots of the ratio I_M/I_{M_0} versus magnetic field are given in Fig. 4 for various sodium densities. To compare the field dependences obtained at various densities, we normalize the ratios I_M/I_{M_0} at fields between 4 and 6 kG. Such plots may be seen on Figs. 5 and 6. The observed pa-

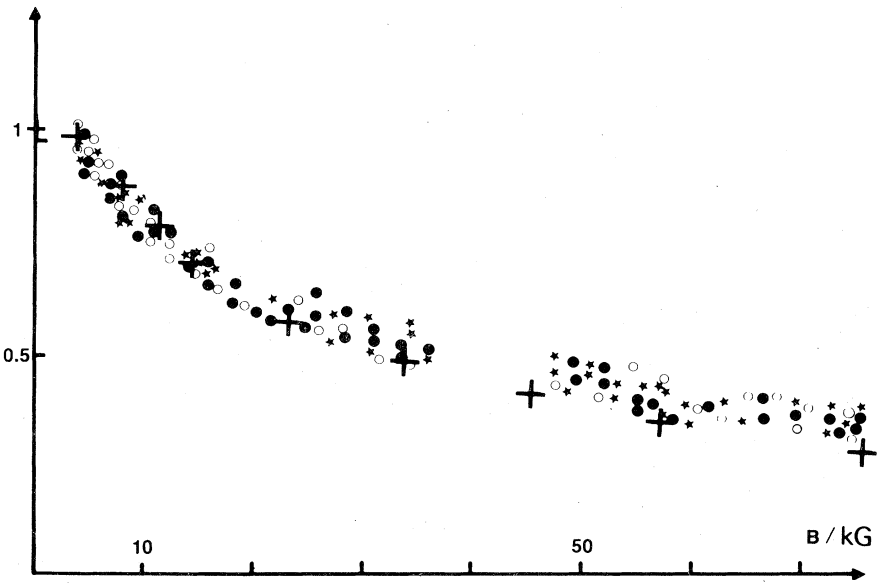

FIG. 6. Variation with the field of $\eta^{1/2-1/2} = \rho^{1/2-1/2}(B) / \rho^{1/2-1/2}(B_0)$ (with $B_0 = 4$ kG) for various values of the density: $N = 4.2 \times 10^{12}$ at./cm^3 (○), $N = 3.4 \times 10^{12}$ at./cm^3 (★), and $N = 2.9 \times 10^{12}$ at./cm^3 (●). The theoretical values (+) are those predicted for $g^{1/2-1/2}(B) / g^{1/2-1/2}(B_0)$ with the use of the correlation function for R^{-3} dipole-dipole interaction.

rameter is then[1]

$$\eta^{MM_0}=\frac{\lambda^M(N,B)}{\lambda^M(N,B_0)}\frac{\lambda^{M_0}(N,B_0)}{\lambda^{M_0}(N,B)}\frac{\Gamma^M(N,B_0)}{\Gamma^M(N,B)}\frac{g^{MM_0}(B)}{g^{MM_0}(B_0)}. \tag{8}$$

The dispersion of the data with density is in general very small, verifying that $\eta(B)$ is nearly independent of N, as it should be.

As there is no possibility of decoupling effects in the $M=-\frac{3}{2}\rightarrow\frac{3}{2}$ case, the plot of $\eta(B)$ in Fig. 5 is free from field effects on radiation trapping, so one has

$$\eta^{(3/2-3/2)}=g^{3/2-3/2}(B)/g^{3/2-3/2}(B_0), \tag{9}$$

with $B_0=6$ kG. The field dependence observed between 6 and 80 kG is about a factor of 20.[21] The interpretation of this feature is given in Sec. VII.

The field dependence of the $J=\frac{1}{2}M=-\frac{1}{2}\rightarrow M=\frac{1}{2}$ case is about a factor of 3 between 4 and 80 kG; this may be partly due to LS decoupling effects acting on the parameters of radiation trapping. An estimate of the magnitude of this effect can be obtained as follows. Using the results of Appendix A, at low densities, one has

$$I^{1/2\,1/2}/I^{1/2-1/2}\sim(g^{1/2-1/2}/\Gamma)(1+\tfrac{8}{9}\mu_B B/A),$$

where A is the fine-structure constant. From this expression, we see that $\vec{L}\cdot\vec{S}$ decoupling effects lead to a 30% increase in the ratio of the measured intensities between 0 and 80 kG. However, this first-order correction may not be very accurate, since the effects of multiple scattering are certainly nonlinear in the absorption coefficient within the density range of the experiments. Indeed, the data indicate that the net effect of the field dependence of the multiple-scattering parameters is less than this. The values of $\eta^{1/2-1/2}$ plotted in Fig. 6 reveal that the dispersion of the data for various values of the density is very weak. As multiple-scattering parameters depend nonlinearly on the absorption coefficient and thus on field strength and density, a strong field dependence would result in a strong dispersion of the data with N, which is not consistent with the plot of Fig. 6. It is thus highly probable that the field dependence in η due to decoupling effects and multiple scattering is weak and not greater than 20% over the whole 4–80 kG range of magnetic field. The main part of the observed variation is thus due to the effect of the field on the collision rate.

VII. APPROXIMATE THEORY FOR Na-Na* COLLISIONS

A. Generalities

The zero-field problem has been solved in Ref. 5, a good approximation which neglects fine-structure transitions. A treatment of the collision problem in strong fields must take into account both magnetic and $\vec{L}\cdot\vec{S}$ interactions, as crossings of fine-structure Zeeman sublevels occur at 164 and 250 kG and decoupling effects are no longer negligible (see Fig. 7). The general solution of the relaxation problem for Na-Na* resonant collisions must solve a 24×24 set of coupled first-order differential equations. The use of symmetry properties does not afford simplifications. In contrast to the zero-field situation, there is no possibility of splitting the set of equations into several subsets of smaller dimensions.[5] One has then to solve the (24 by 24) set for each value of (ϕ,θ,γ), B, b, and v following the methods of Ref. 22, which requires a prohibitive amount of computer time. Approximations are thus needed.

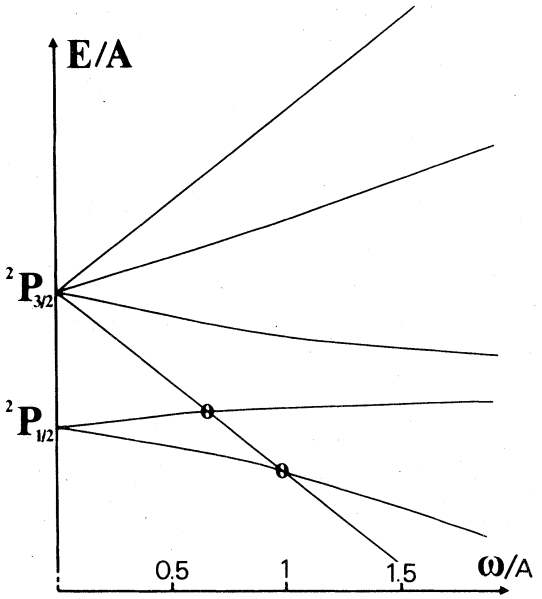

FIG. 7. Fine-structure energy diagram of the Na 3^2P state as a function of the magnetic field with ω/A the ratio of Larmor frequency to the fine-structure constant. The crossings of energy levels occur at 164 kG and 245 kG. The assignment of the value of M on energy levels is obvious from the low-field Zeeman pattern.

B. Approximate theory

The principle of the method is described in Refs. 4, 12, and 15. A second-order expansion of the relaxation matrix is performed in an interaction potential V supposed to be that of an R^{-3} dipole-dipole interaction. The transfer rates are then derived by means of a cutoff method. As there are two possible polarization states for the perturber before and after the collision process, the probability of excitation transfer will be written

$\Pi^{(j_1m_1,j_2M_2)(J_1M_1,j_2m_2)}$, where (jm) denotes ground substates and (JM) excited substates. The general form of the Π coefficients from Appendix B is then

$$\Pi^{(j_1m_1,j_2M_2)(J_1M_1,j_2m_2)} = q^2 f_1(\eta_0) K(\{a\}), \qquad (10)$$

with $q = p/(b^2v) = \frac{9}{4}\,\Gamma/(k_0^3 b^2 v)$ and

$$\eta_0 = (b/v)[g_f(m_2 - m_1)\omega + E(J_1M_1) - E(J_2M_2)].$$

The K function involves a sum over angular factors and depends on the $\{a\}$ coefficients, which describe decoupling effects due to the field; the explicit expression for K is given in Appendix B. In Eq. (10) f_1 is the Fourier transform of the symmetrical correlation function of the R^{-3} dipole-dipole interaction.[12,22]

Equation (10) allows us to point out two possible origins of the field dependence of the Π coefficients (from the second-order theory). The first comes from the $\{a\}$ coefficients and is due to decoupling effects during collision. It is not of fundamental interest as concerns the mechanism, but may explain in some cases[10,23] the appearance of strong variations with the field, for example, if a mixing of a small cross section with a large one occurs. These mixing effects in the present cases are always small for $B < 80$ kG, and in general are no more than 10% of the zero-field cross sections (see Appendix I). The second origin of the field dependence, which is primarily of interest, comes from the $f_1(\eta_0)$ function. Note that at this order of perturbation theory the two effects are not coupled. The argument η_0 of f_1 depends only on the energy difference between the initial and final states of the two-atom system (see Fig. 8), showing the very important role played by the polarizations and energies of the perturbers in the ground sublevels. When no decoupling of L and S by the field occurs, $f_1(\eta_0)$ is the only term in (10) which depends on the field strength. Equation (10) also permits us to predict the order of magnitude of angular terms. The summation in K is 0 when one of the rules for selection of Clebsch-Gordan coefficients is not fulfilled. Indeed, in this second-order theory, they only express the electric dipolar selection rules obeyed by dipole-dipole interaction for each atom. One can then easily show that some transfer processes are forbidden in second-order perturbation theory. They may of course take place at higher orders, but they will be one order of magnitude smaller than the allowed processes in second order. By the use of (10) one may thus test directly the symmetry properties of the interaction potential.

In a strong magnetic field symmetries obtained in second order are larger than the true ones obtained in Ref. 12. As has been mentioned, the relation between the M and $-M$ transfer rates break down when decoupling effects are taken into account.

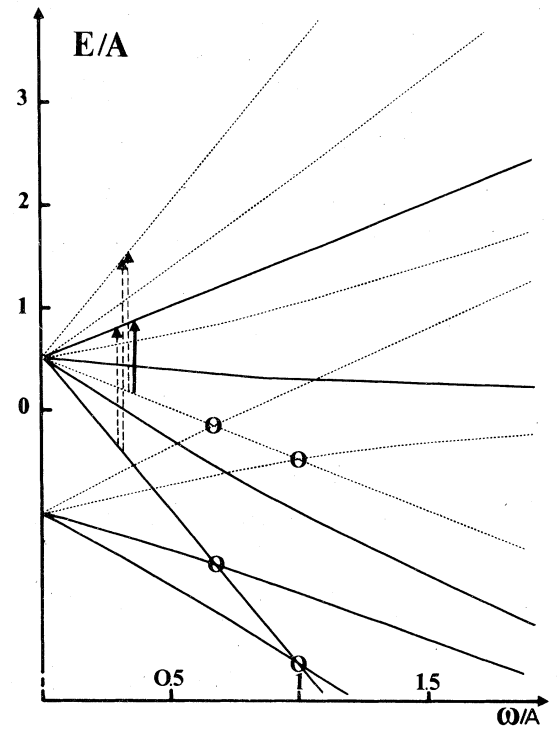

FIG. 8. Energy diagram for the two-atom Na*-Na system plotted against ω/A. The first atom is in the $|3\,^2P, JM_J\rangle$ excited sublevel. The second atom is in the $|j=\frac{1}{2}, m_j\rangle$ ground sublevel. The energy levels are labeled by (M_J, m_j). The full curves correspond to $m_j = -\frac{1}{2}$ ground states, and dashed curves to $m_j = +\frac{1}{2}$ ground substates. The value of M_J can be easily deduced from the low-field Zeeman pattern. Several crossings of energy levels (at 86, 103, 124, 164, 172, and 245 kG) occur in the two-atom system, corresponding to a zero in the energy difference between the initial and final state in the collision processes. They may also correspond to resonances in high field of the collisional transfer rates. The energy diagram gives directly the energy difference involved for a given excitation-transfer process and the rate of variation with the field strength. The four diffusion amplitudes *a priori* contributing to the $M = -\frac{3}{2} \rightarrow M = \frac{3}{2}$ excitation transfer in the excited state are represented on the figure at arbitrary field value. The dashed arrows are in fact collisional transitions forbidden at second order because of dipole-dipole selection rules.

The whole set of $\{\Pi\}$ coefficients is given in Appendix B, where we indicate some extensions of symmetry properties applicable only in second-order perturbation theory.

C. Mean excitation transfer probability in excited state

The existence of a structure in the ground state allows the possibility of various effects such as

collisional pumping via resonant collisions. Under our conditions, the number of excited atoms is always very small and such effects are negligible. Following Sec. V, ground-state atoms are on the average unpolarized and well described by the density matrix

$$\rho_g \simeq \tfrac{1}{2}\sum_m |\tfrac{1}{2}m\rangle\langle\tfrac{1}{2}m| . \tag{11}$$

The mean excitation-transfer probability from (J_1M_1) to (J_2M_2) in the excited state is

$$\Pi^{(J_2M_2)(J_1M_1)} = \tfrac{1}{2}\sum_{m_1m_2} \Pi^{(j_1m_1,\,J_2M_2)(J_1M_1,\,j_2m_2)} . \tag{12}$$

Each experimentally observed process in the excited state is a superposition of four processes for the two-atom system, which differ by the polarization of the ground-state atoms before and after collision. These four processes correspond, moreover, to various energy differences in the energy diagram of Fig. 8, given by

$$\Delta E(J_1M_1, J_2M_2) = [g_f(m_2 - m_1)\omega + E(J_1M_1) - E(J_2M_2)] , \tag{13}$$

with $m_2, m_1 = \pm\frac{1}{2}$.

The mean excitation-transfer probability between (J_1M_1) and (J_2M_2) then usually varies with the field strength at four characteristic frequencies, owing to the energy differences (13). The field dependence of the collisional transfer may give some insight into the contributions of these various processes to electronic excitation transfer in the excited state, as they generally have different rates of variation. If some contributing processes are forbidden, this will result in the absence of data for the corresponding frequencies. One is thus able to test the symmetry properties of the interaction potential.

Note that varying the field is in some aspects equivalent to performing a Fourier analysis of the correlation function of the potential.[12]

The preceding clearly reveals the importance of the role of electronic spin in the collisional process although the interaction potential is of purely orbital nature. This role is manifest in the modifications of the energy levels of the two-atom system, in the selection rules, and also in the two polarization states of the perturbers resulting in four different processes contributing to transfer in the excited state.

D. Dependence of transfer rates on field strength

The deduction of the transfer rates is made following the method of,[12] by using a cutoff procedure and the mean transfer probability of Eq. (12). As remarked in Refs. 1, 12, and 21, this only gives an order of magnitude for the variation of the transfer rate with the field. The role of *LS* decoupling effects during the collision time is almost negligible for the evaluation of the variations with the field. It causes at most a 20% supplementary variation in the 0–80 kG range of field strength. The departure of energies from the Zeeman approximation can be shown to be of no practical importance over the same range of fields. Thus we neglect these effects. The cutoff radius are obtained from the exact computed values in zero field given in,[5] by assuming the identity of the cross sections obtained either by numerical analysis or by the cutoff method, in zero field. The transfer rates are then given by[12]

$$\frac{g(B)}{g(0)} = \Phi(B) = \frac{1}{2}\frac{\eta_c^2}{\tau^2}\left[1 + \left(\frac{\tau}{\eta_c}\right)^4 \sum_i a_i F(\alpha_i\eta_c)\right] , \tag{14a}$$

$$\sum_i a_i f_1(\alpha_i\eta_c) = \frac{\eta_c^4}{\tau} , \tag{14b}$$

$$\tau = \omega[p\mu^{1/2}/v^3]^{1/2} , \tag{14c}$$

where f_1 and F are defined in Refs. 12 and 22. The $(JM \to J'M')$ dependence is implicit, $\{a_i, \alpha_i\}$ are some angular factors, and τ is proportional to the magnetic field and is just the adiabaticity parameter for R^{-3} dipole-dipole interaction. Equation (14b) allows the determination of the cutoff radius b_c and then of the quantity η_c such that $\eta_c \sim (\Delta E/\hbar)(b_c/v)$, where ΔE is given by (13). Then (14a) just gives the value of the transfer rate. Many more details can be obtained from Ref. 12.

From (10) and (14) it is easy to deduce the general behavior with the field of all the transfer coefficients. For fine-structure transfer coefficients, or strong field values (≫80 kG), it is necessary to include *LS* decoupling effects, which would slightly affect the general form of Eq. (14).

In the $(-\frac{3}{2} \to \frac{3}{2})$ excitation-transfer case, Eq. (14) explicitly gives

$$\Phi(B) = \frac{g^{3/2-3/2}(B)}{g^{3/2-3/2}(0)} = \frac{1}{2}\frac{\eta^2}{\tau^2}\left(1 + \frac{\tau^4}{\eta^4}F(2\eta)\right) ,$$

$$\eta^4/\tau^4 = f_1(2\eta), \quad \eta = \omega b/v ,$$

and $\tau = 0.106B$ kG. The Φ function can be obtained from Table I of Ref. 12.

The rate of variation of $g^{3/2-3/2}$ with the field is governed by the factor $2\mu_B B$, a fact which requires comment. In general, as mentioned above, four processes, differing by the polarizations of ground-state atoms, contribute to excitation transfer in the excited state, assuming unpolarized ground-state perturbers on the average. But for the $M = -\frac{3}{2} \to M = \frac{3}{2}$ excitation-transfer process, three among these are forbidden in second-order pertur-

TABLE I. Fluorescence-intensity ratio I_D/I_E for $B=80$ kG normalized at the value for $B=0$ kG.

I_E \ I_D	$\tilde{\frac{3}{2}}\frac{3}{2}$	$\tilde{\frac{3}{2}}\frac{1}{2}$	$\tilde{\frac{3}{2}}-\frac{1}{2}$	$\tilde{\frac{3}{2}}-\frac{3}{2}$	$\tilde{\frac{1}{2}}\frac{1}{2}$	$\tilde{\frac{1}{2}}-\frac{1}{2}$
$\tilde{\frac{3}{2}}\frac{3}{2}$	1	0.73	1.27	1	1.13	0.87
$\tilde{\frac{3}{2}}\frac{1}{2}$	1.27	1	1.54	1.27	1.40	1.14
$\tilde{\frac{3}{2}}-\frac{1}{2}$	0.73	1.54	1	0.73	0.86	0.60
$\tilde{\frac{3}{2}}-\frac{3}{2}$	1	0.73	1.27	1	1.13	0.87
$\tilde{\frac{1}{2}}\frac{1}{2}$	0.87	0.60	1.14	0.87	1	0.73
$\tilde{\frac{1}{2}}-\frac{1}{2}$	1.13	0.87	1.40	1.13	1.27	1

bation theory because of the electric dipolar selection rules obeyed by the dipole-dipole interaction. The only term which is not zero corresponds to the $(M=-\frac{3}{2}, m=\frac{1}{2} \rightarrow M=\frac{3}{2}, m=-\frac{1}{2})$ process, meaning that the spin of ground-state atoms is reversed during the collision. Then evolution of $g^{3/2-3/2}$ is dependent on only one characteristic frequency, which is just $2\mu_B B$.

If one neglects the role of the electronic spin of the ground-state perturber in the collision, one would predict a rate of variation with B corresponding to the splitting of the $(-\frac{3}{2})$ and $(+\frac{3}{2})$ Zeeman sublevels of the excited state, i.e., $4\mu_B B$. This indeed refers to a process strictly forbidden here, but in Na*–rare-gas collisions the only one.[9]

In the $(\frac{1}{2}-\frac{1}{2} \rightarrow \frac{1}{2}\frac{1}{2})$ excitation-transfer case, Eq. (14) does give

$$\Phi(\tau)=\frac{g(B)}{g(0)}=\frac{1}{2}\frac{\eta^2}{\tau^2}\left\{1+\frac{\tau^4}{\eta^4}\left[\tfrac{3}{10}F(\tfrac{2}{3}\eta)+\tfrac{1}{10}F(\tfrac{4}{3}\eta)+\tfrac{3}{5}F(\tfrac{8}{3}\eta)\right]\right\},$$

$$\tau=\eta\left[\tfrac{3}{10}f(\tfrac{2}{3}\eta)+\tfrac{1}{10}f(\tfrac{4}{3}\eta)+\tfrac{3}{5}f(\tfrac{8}{3}\eta)\right]^{-1/4},$$

with $\tau=0.076B$ kG.

In this case, there are really four processes contributing to excitation transfer in the excited state, with different weights and different rates of variation with the field strength.

E. Comparison with experimental results

For $(-\frac{3}{2} \rightarrow +\frac{3}{2})$ excitation transfer, the experimental and theoretical results are plotted in Fig. 5, and agreement is fairly good. It clearly shows that the rate of variation of $g^{3/2-3/2}$ is well described by $2\mu_B B$ and not by $4\mu_B B$, which would produce a faster decrease with the field. The large field dependence experimentally observed illustrates the importance of the collision time and correlation time of the potential in resonant collisions. The good overall agreement with the theoretical model confirms both the importance of the role of selection rules and electronic spin in Na-Na* collisions. The nearly complete elimination of the long-range R^{-3} contributions to excitation transfer in strong fields suggests the possibility of studying the effects of the higher-order, nonresonant terms of the potential, which are masked in zero fields by the resonant contribution. However, the zero-field cross section from theoretical evaluations[5] is about 8400 Å^2 for $(-\frac{3}{2} \rightarrow \frac{3}{2})$ excitation transfer, so that a high-field limit of 400 Å^2 is then deduced from our results. This is still fairly large compared to Na-Ne cross sections,[9] which probably represent the order of magnitude of the nonresonant contributions in Na-Na* collisions as well.

For $(\frac{1}{2}-\frac{1}{2} \rightarrow \frac{1}{2}-\frac{1}{2})$ excitation transfer, the agreement is also very good, further indicating that the field dependence arising from LS decoupling and multiple-scattering effects is really very small. The role of the three different rates of variation with the field associated with the four contributing processes can be seen from the curve: the rapid decrease between 4 and 20 kG is due to the term at frequency $\frac{8}{3}\omega$ which corresponds to the $(\frac{1}{2}M=-\frac{1}{2}, \frac{1}{2}m=-\frac{1}{2} \rightarrow \frac{1}{2}m=\frac{1}{2}, \frac{1}{2}M=\frac{1}{2})$ process in the two-atom system. This term becomes negligibly small at 20 kG. For $B>30$ kG the residual transfer rate is given within 1% by the term at frequency $\frac{2}{3}\omega$, which is slowly varying with the field and almost constant between 0 and 20 kG. It corresponds to the $(\frac{1}{2}M=-\frac{1}{2}, \frac{1}{2}m=\pm\frac{1}{2} \rightarrow \frac{1}{2}m=\pm\frac{1}{2}, \frac{1}{2}M=\frac{1}{2})$ processes.

VIII. CONCLUSIONS

The use of strong magnetic fields to analyze the behavior of the cross sections with the energy difference between the levels in atom-atom collisions permits direct confirmation of the main mechanisms of resonant collisions. A simple theoretical approach using the Fourier transform of the cor-

relation function for R^{-3} dipole-dipole interaction is shown to be in good agreement with the experimental data obtained in a vapor. This confirms over a wide range of frequencies the R^{-3} dependence of the potential. No significant contributions to excitation transfer of higher-order terms of the potential have been shown. Also, direct experimental confirmation of the validity of electric dipolar selection rules for the interaction has been given. The rate of variation with the field for the various contributing processes are shown to be different. An almost complete elimination at strong field of some of the processes is then possible. In some cases this means one can perform experiments with polarized perturbers in a thermalized vapor, since only one class of ground-state atoms will interact with the excited atoms in a strong field.

APPENDIX A: $\vec{LS}$ DECOUPLING EFFECTS

The Hamiltonian $\mathcal{H}_e$ in the excited state is given by

$$\mathcal{H}_e = A\vec{L}\cdot\vec{S} + \mu_B(\vec{L}+2\vec{S})\cdot\vec{B}\,.$$

The eigenvectors of $\mathcal{H}_e$ in the $|LSJM\rangle$ basis are then

$$|\tilde{J}M\rangle = \sum_{J'} a(JJ'M)|LSJM\rangle\,, \qquad \text{(A1)}$$

and the $\{a\}$ coefficients are given by

$$a(\tfrac{3}{2}\tfrac{3}{2}\pm\tfrac{1}{2}) = \cos\tfrac{1}{2}\theta_\pm\,,\quad a(\tfrac{3}{2}\tfrac{1}{2}\pm\tfrac{1}{2}) = \sin\tfrac{1}{2}\theta_\pm\,,$$
$$a(\tfrac{1}{2}\tfrac{3}{2}\pm\tfrac{1}{2}) = -\sin\tfrac{1}{2}\theta_\pm\,,\quad a(\tfrac{1}{2}\tfrac{1}{2}\pm\tfrac{1}{2}) = \cos\tfrac{1}{2}\theta_\pm\,,$$

with

$$\tan\tfrac{1}{2}\theta_\pm = -\tfrac{2}{3}\sqrt{2}\,\omega/(\tfrac{3}{2}A\pm\tfrac{1}{3}\omega)\,,\quad \omega = \frac{\mu_B B}{\hbar}$$

and A the fine-structure constant. The associated eigenvalues are

$$E(\tilde{\tfrac{3}{2}}\pm\tfrac{3}{2}) = \tfrac{1}{2}A \pm 2\omega\,,$$
$$E(\tilde{\tfrac{3}{2}}\pm\tfrac{1}{2}) = \tfrac{1}{2}[(\pm\omega - \tfrac{1}{2}A) + (\omega^2 \pm A\omega + \tfrac{9}{4}A^2)^{1/2}]\,,$$
$$E(\tilde{\tfrac{1}{2}}\pm\tfrac{1}{2}) = \tfrac{1}{2}[(\pm\omega - \tfrac{1}{2}A) - (\omega^2 \pm A\omega + \tfrac{9}{4}A^2)^{1/2}]\,.$$

The intensities of the lines connecting the $|\tilde{J}M\rangle$ and the ground $|jm_j\rangle$ substates in the electric dipolar approximation depend on the field strength and are given by

$$I(\tilde{J}M_J \to jm_j) = |\langle l=0\, s=\tfrac{1}{2}\, j=\tfrac{1}{2}m_j|R|L=1\, S=\tfrac{1}{2}\tilde{J}M_J\rangle|^2\,,$$

with

$$\langle 0\tfrac{1}{2}\tfrac{1}{2}\|R\|1\tfrac{1}{2}J\rangle = \langle 0\|R\|1\rangle(-)^{J+3/2} \times (2J+1)^{1/2}\sqrt{2}\begin{Bmatrix} 0 & 1 & 1 \\ J & \frac{1}{2} & \frac{1}{2}\end{Bmatrix}.$$

Writing $p = \frac{1}{3}|\langle l=0\|R\|L=1\rangle|^2$, one obtains for the intensities of the σ and π lines (units of p)

	σ	π
$\tilde{\frac{3}{2}}\frac{3}{2}$	1	0
$\tilde{\frac{3}{2}}\frac{1}{2}$	$\frac{1}{3}(\cos\frac{1}{2}\theta_+ + \sqrt{2}\sin\frac{1}{2}\theta_+)^2$	$\frac{2}{3}(\cos\frac{1}{2}\theta_+ - 2^{-1/2}\sin\frac{1}{2}\theta_+)^2$
$\tilde{\frac{3}{2}}-\frac{1}{2}$	$\frac{1}{3}(\cos\frac{1}{2}\theta_- - \sqrt{2}\sin\frac{1}{2}\theta_-)^2$	$\frac{2}{3}(\cos\frac{1}{2}\theta_- + 2^{-1/2}\sin\frac{1}{2}\theta_-)^2$
$\tilde{\frac{3}{2}}-\frac{3}{2}$	1	0
$\tilde{\frac{1}{2}}\frac{1}{2}$	$\frac{2}{3}(\cos\frac{1}{2}\theta_+ - 2^{-1/2}\sin\frac{1}{2}\theta_+)^2$	$\frac{1}{3}(\cos\theta\frac{1}{2}\theta_+ + \sqrt{2}\sin\frac{1}{2}\theta_+)^2$
$\tilde{\frac{1}{2}}-\frac{1}{2}$	$\frac{2}{3}(\cos\frac{1}{2}\theta_- + 2^{-1/2}\sin\frac{1}{2}\theta_-)^2$	$\frac{1}{3}(\cos\frac{1}{2}\theta_- - \sqrt{2}\sin\frac{1}{2}\theta_-)^2$

for $B \leq 80$ kG, $\theta_\pm \ll 1$, and $\theta_+ \sim \theta_- \sim \frac{4}{9}\sqrt{2}\,\omega/A$.

This leads to the simplified expressions

σ	π
1	0
$\frac{1}{3}(1+\sqrt{2}\,\theta_+)$	$\frac{2}{3}(1-\theta_+/\sqrt{2})$
$\frac{1}{3}(1-\sqrt{2}\,\theta_-)$	$\frac{2}{3}(1+\theta_-/\sqrt{2})$
1	0
$\frac{2}{3}(1-\theta_+/\sqrt{2})$	$\frac{1}{3}(1+\sqrt{2}\theta_+)$
$\frac{2}{3}(1+\theta_-/\sqrt{2})$	$\frac{1}{3}(1-\sqrt{2}\,\theta_-)$.

The intensities of the lines are field dependent, but at all orders in the field one has

$$I^\sigma(J\tilde{M}) + I^\pi(J\tilde{M}) = \text{const.}$$

For the isolated atom, the ratio I_D/I_E of the fluorescence intensities for $B = 80$ kG normalized at the value for $B = 0$ kG are given in Table I.

APPENDIX B: EXPLICIT EXPRESSION OF π COEFFICIENTS

The principle of the derivations is to use second-order perturbation theory to express the relaxation matrices for the two-atom system. We restrict the analysis to population transfer. Defining

$$\mathcal{H}_f = g_f\omega m_j = 2\mu_B\vec{S}\cdot\vec{H}$$

as the Zeeman Hamiltonian of ground-state atoms, $\mathcal{H}_e$ as the Hamiltonian for the excited state, and

$P(X)$ as the R^{-3} dipole-dipole interaction, one obtains

$$S_2 = -i\int_{-\infty}^{+\infty} \exp\left(i\frac{bx}{v}(\mathcal{H}_{f_1}+\mathcal{H}_{e_2})\right)P(x)\exp\left(-i\frac{bx}{v}(\mathcal{H}_{e_1}+\mathcal{H}_{f_2})\right)dx\,,$$

$$S_1 = 1 - \int_{-\infty}^{+\infty}\int_{-\infty}^{x} \exp\left(i\frac{bx}{v}(\mathcal{H}_{e_1}+\mathcal{H}_{f_2})\right)P(x)\exp\left(-i\frac{bx}{v}(\mathcal{H}_{f_1}+\mathcal{H}_{e_2})\right)$$
$$\times\exp\left(i(\mathcal{H}_{f_1}+\mathcal{H}_{e_2})\frac{bx'}{v}\right)P(x')\exp\left(-i\frac{bx'}{v}(\mathcal{H}_{e_1}+\mathcal{H}_{f_2})\right)dx\,dx'\,.$$

The relaxation rates are calculated in the eigenvector basis of $\mathcal{H}_e$, giving (with evident definitions)

$$\Pi^{(\tilde{J}_1'M_1', j_2m_2';\tilde{J}_1M_1)(j_2m_2)}(\tilde{J}_1M_1, j_2m_2;\tilde{J}_1M_1, j_2m_2)(i) = \delta_{i_1}\delta_{m_2'm_2}\delta_{M_1'M_1}$$
$$-\operatorname{tr}\{|J_1'M_1'j_2m_2'\rangle\langle J_1'M_1', j_2m_2'|^{\dagger}S_i|J_1\tilde{M}_1, j_2m_2\rangle\langle J_1\tilde{M}_1, j_2m_2|S_i^{+}\}_{\mathrm{ANG}}$$

for excitation transfer of the populations.

At second order, one can easily show that $\Pi(1)=0$ and $\Pi(2)\neq 0$, since

$$\Pi^{(j_1m_1,\tilde{J}_2M_2)(\tilde{J}_1M_1, j_2m_2)} = -\{|\langle j_1m_1, \tilde{J}_2M_2|S_2|\tilde{J}_1M_1, j_2m_2\rangle|^2\}_{\mathrm{ANG}}\,.$$

The angular average is obtained by expanding the $|\tilde{J}M\rangle$ states over the $|JM\rangle$ basis. One then obtains straightforwardly

$$\Pi^{(j_1m_1,\tilde{J}_2M_2)(\tilde{J}_1M_1, j_2m_2)}$$
$$= \frac{4}{45}\left\{\frac{|\langle 0\|P\|1\rangle|^2}{b^2v}\right\}^2 f_1(\eta_0)\sum_{\substack{J_1'J_1''\\ J_2'J_2''}}(-)^{2J_1'+2J_1''+J_2'+J_2''}(2J'+1)^{1/2}(2J_1''+1)^{1/2}$$
$$\times a(J_1J_1'M_1)a(J_2J_2'M_2)a(J_1J_1''M_1)a(J_2J_2''M_2)\langle 2q|11q_1q_2\rangle^2\langle j_1m_1|J_1'1M_1q_1\rangle$$
$$\times\langle J_2'M_2|j_21m_2q_2\rangle\langle j_1m_1|J''1M_1q_1\rangle\langle J_2''M_2|j_21m_2q_2\rangle\,, \qquad \text{(B1)}$$

with

$$\eta_0 = (b/v)[g_f(m_2-m_1)\omega + E(\tilde{J}_1M_1) - E(\tilde{J}_2M_2)]$$

and $f_1(\eta)$ the Fourier transform of the correlation function for R^{-3} dipole-dipole interaction. This general expression shows that the Π coefficients in second order depend on the field strength in two different ways. The values of the coefficients obtained in (B1) are linked with symmetry properties given in Ref. 12. Fine-structure transitions obey the symmetry properties of Ref. 12, provided one changes A to $-A$ in the $f_1(\eta_0)$ function when changing $\{M\}$ in $-\{M\}$. From (A2) one can deduce the expressions for fine-structure transfer coefficients. Specifically this gives after averaging over the ground-state sublevels

$$\bar{\Pi}(\tfrac{3}{2}-\tfrac{3}{2})(\tfrac{1}{2}-\tfrac{1}{2}) = -\frac{2}{135}\left\{\frac{\langle 0\|P\|1\rangle}{b^2v}\right\}^2\left[(\cos\tfrac{1}{2}\theta_- - \sqrt{2}\sin\tfrac{1}{2}\theta_-)^2 f_1\left(\frac{b}{v}[E(\tfrac{3}{2}-\tfrac{3}{2})-E(\tfrac{1}{2}-\tfrac{1}{2})]\right)\right.$$
$$\left.+\tfrac{2}{3}(\cos\tfrac{1}{2}\theta_- + 2^{-1/2}\sin\tfrac{1}{2}\theta_-)^2 f_1\left(\frac{b}{v}[2\omega+E(\tfrac{3}{2}-\tfrac{3}{2})-E(\tfrac{1}{2}-\tfrac{1}{2})]\right)\right],$$

$$\bar{\Pi}(\tfrac{3}{2}-\tfrac{3}{2})(\tfrac{1}{2}\pm\tfrac{1}{2}) = -\frac{2}{135}\left\{\frac{\langle 0\|P\|1\rangle}{b^2v}\right\}^2\left[4(\cos\tfrac{1}{2}\theta_+ - 2^{-1/2}\sin\tfrac{1}{2}\theta_+)^2 f_1\left(\frac{b}{v}[E(\tfrac{3}{2}-\tfrac{3}{2})-E(\tfrac{1}{2}\tfrac{1}{2})]\right)\right.$$
$$\left.+(\cos\tfrac{1}{2}\theta_+ + \sqrt{2}\sin\tfrac{1}{2}\theta_+)^2 f_1\left(\frac{b}{v}[2\omega+E(\tfrac{3}{2}-\tfrac{3}{2})-E(\tfrac{1}{2}\tfrac{1}{2})]\right)\right].$$

Then, using the methods of Ref. 12, one can easily deduce the variations with field strength of the transfer coefficients, particularly the behavior around the crossing points in the two-atom energy diagram (cf. Fig. 8).

*Universität Marburg (R.F.A.).
†Associé au Centre National de la Recherche Scientifique—Laboratoire No. 18.

[1a]J. C. Gay and W. B. Schneider, J. Phys. (Paris) Lett. 36, L185 (1975).
[1b]J. C. Gay and W. B. Schneider, Phys. Rev. A 20, 894 (1979).
[1c]L. Krause, *The Excited State in Chemical Physics*, edited by J. W. McGowan (Wiley, New York, 1975).
[2]J. Pitre and L. Krause, Can. J. Phys. 45, 2671 (1967).
[3]H. L. Chen and S. Fried IEEE J. Quantum Electron 8, 252 (1975).
[4]J. C. Gay, thesis, University of Paris, 1976 (unpublished).
[5]C. G. Carrington, D. N. Stacey, and J. Cooper, J. Phys. B 6, 417 (1973).
[6]T. Holstein, Phys. Rev. 72, 1212 (1947).
[7]J. C. Gay and A. Omont, (unpublished).
[8]A. Omont and J. Brossel, C. R. Acad. Sci. 252, 710 (1961); A. Omont, thesis, University of Paris, 1961 (unpublished).
[9]J. C. Gay and W. B. Schneider, Z. Phys. A 278, 211 (1976).
[10]J. Guiry and L. Krause, Phys. Rev. A 12, 2407 (1975).
[11]E. U. Condon and G. H. Shortley, *The Theory of Atomic Spectra*, Cambridge, 1935.
[12]J. C. Gay and W. B. Schneider, Phys. Rev. A 20, 879 (1979).
[13]M. I. Diakonov and V. I. Perel, Sov. Phys. JETP 20, 997 (1965).
[14]W. Happer, Rev. Mod. Phys. 44, 169 (1972).
[15]A. Omont, Progr. Quantum Electron 5, 69 (1977).
[16]M. A. Bouchiat, thesis, University of Paris, 1965 (unpublished).
[17]F. Grossetête, thesis, University of Paris, 1967 (unpublished).
[18]A. Moretti and F. Strumia, Phys. Rev. A 3, 349 (1971).
[19]F. A. Franz, T. R. Marshall, and J. A. Munarin, Phys. Lett. 36, 31 (1971).
[20]W. Happer, Phys. Rev. B 1, 2203 (1970).
[21]J. C. Gay and W. B. Schneider, Phys. Lett. A 62, 403 (1977).
[22]J. C. Gay, J. Phys. (Paris) 37, 1135 (1976).
[23]W. E. Baylis, *Progress in Atomic Spectroscopy*, edited by W. Hanle and H. Kleinpoppen (Plenum, New York, 1978), Pt. A, Vol. II.